

Study of different materials response in micro milling using four edged micro end mill tools

Ganesh Malayath, Ajay M. Sidpara*, Sankha Deb

Mechanical Engineering Department, Indian Institute of Technology Kharagpur, Kharagpur, India

ARTICLE INFO

Keywords:

Micro milling
End mill tools
Burr formation
Surface roughness

ABSTRACT

Fabrication of micro channels with a width of less than 200 μm is always challenging as the available cutting tools are costly and not adequate for machining for a longer time. Popular tool fabrication processes like tool grinding experience high scrap rate as the micro features in the cutting tools cannot withstand the grinding forces. Other non-contact tool fabrication processes like focused ion beam machining (FIB) and wire electro-discharge machining (wire EDM) are very slow and need high capital investment. In this paper, micro end mill tools with high dimensional accuracy are fabricated by a sequential EDM method and the performance analysis is conducted by milling micro channels of different depth on aluminium 6061, brass 340, AISI 1040 and poly methyl methacrylate (PMMA). The cutting tools are proven to be capable of producing micro channels of high dimensional accuracy ($100 \pm 4 \mu\text{m}$), nanometer surface finish (29–120 nm), high surface integrity, and less post-milling tool damages.

1. Introduction

Microchannel fabrication is a necessary step in various applications in electronics, biomedical, aerospace industries, etc. For example, integrated methanol fuel processors use steel microchannel patterned devices to equip the polymer electrolyte membrane fuel cell as an alternative to conventional batteries [1]. Micro reactors use channeled metallic platelets stacks coated with active catalysts which ensure compactness, rapid mass and heat transfer, reduced pressure drop compared to packed bed reactors and greater thermal stability [2]. For cooling of microelectronic devices, a brass honeycomb micro channel system is developed [3]. Aluminum bipolar plates with micro channels are used in proton exchange membrane fuel cells [4]. Micro channels are an inevitable part of polymer microfluidic devices, including micro mixers [5] and devices for detection and isolation of circulating tumor cells [6], etc.

Among the various technologies used for microchannel fabrication, injection molding [7], laser micromachining [8], stereolithography [9], rubber pad forming [4], contact liquid photolithographic polymerization [10] and selective etching [11] are more popular than the conventional micromachining techniques. Even though conventional machining processes like micro milling promise less fabrication time, high flexibility, mass production environment, and ability to fabricate 3D freeform surfaces with greater accuracy, it gained comparatively less

attention, primarily due to scarcity of adequate cutting tools. In a subtractive machining process, the accuracy and rigidity of cutting tools largely influence the total cost of machining. In the present scenario, the cutting tools used for micromachining are the scaled-down versions of the conventional cutting tools—mostly two flutes flat end mill tools [12] and ball end mill tools [13]. When the diameter of a traditional two flutes end mill tool is reduced beyond 0.5 mm, the core material becomes inadequate to support the cutting edges [14]. Moreover, two flutes tools experience comparatively more chip loading and hammering effect. Due to this, existing micro end mill tools are prone to premature breakage [15,16].

To remove material by shearing and to reduce the negative rake angle during micro milling, the uncut chip thickness (h) has to be greater than a minimum uncut chip thickness (h_{\min}). The value of h_{\min} depends largely on the workpiece material. For AISI 1040, h_{\min} is considered to be 20–35 % of the edge radius [17]. For aluminium, h_{\min} is found to be near to 23 % of the cutting edge radius [18]. Keeping the uncut chip thickness greater than the critical level can be achieved either by increasing the feed per tooth or reducing the cutting edge radius. Increasing the feed per tooth will increase the chip load and tool breakage, especially when the size of the micro tools is less than 200 μm . In traditional micro end mill tool designs, increasing the sharpness of the cutting tool edge may result in weak edges and large stress concentration, which makes it impossible to reduce the edge radius

* Corresponding author.

E-mail address: ajaymsidpara@mech.iitkgp.ac.in (A.M. Sidpara).

beyond a certain value. Additionally, popular tool fabrication methods like tool grinding have the disadvantage of high scrap rate during production, as the tool grinding forces damage the thin micro features on the cutting tools easily.

Non-contact tool fabrication processes for micro end mill tools include focused ion beam machining (FIB) [19], wire EDM [20], wire EDG [21], and block EDM [22]. Micro end mill tools of different geometries with a diameter ranging from 15–100 μm are fabricated using FIB by [23]. However, rounding of the edges close to the ion source and the need for high capital investment make it less attractive to the industry. Wire EDM and wire EDG are successfully used to fabricate polycrystalline diamond micro tools [24–27] but possess very low material removal rate and diamond tools are not cost-effective to be used in micromachining. Malayath et al. [28] proposed a novel micro end mill tool fabrication method based on micro EDM drilling. In this, a cylindrical tool electrode is used to drill holes at specific locations on a cutting tool blank to produce micro end mill tools with 4 cutting edges. Tools with higher dimensional accuracy and shape accuracy is fabricated after finding the optimum EDM parameters for tool fabrication. From the experiments, the micro end mill tool is proved to be having greater rigidity and machining characteristics. As micro EDM drilling is considered to be the fastest among the other EDM variant, the tool fabrication time is much lesser than wired EDM and wire EDG. The method is proven to be suitable for fabricating micro end mill tools with high dimensional accuracy and tool rigidity. However, to exploit the capabilities of the proposed micro end mill tools, machining tests on materials with different mechanical properties have to be conducted.

Most of the microfluidic and microelectronic devices need micro channels of width less than or equal to 100 μm . However, from Table 1, it is clear that cutting tools of 100 μm is rarely used in experimental studies as the tools are prone to easy breakage and are very expensive to fabricate. As the tool rigidity of the cutting tools is very less, the depth cut per pass is restricted to 5–10 % of the cutting tool diameter in all the previous milling experiments. As the cutting edge radius is in the order of 1–5 μm in the end mill tools, the feed per tooth has to be kept very high to reduce the effect of ploughing. Except in some studies with tools fabricated by FIB [29] and block EDM [22], most of the researchers used two flutes cutting tools that experience heavy tool loading and hammering effect compared to four flutes tools. In this paper, the cutting tool design proposed by Malayath et al. [28], is modified for better performance and used to machine micro channels on different materials (aluminium 6061, brass 340, AISI 1040 and poly methyl methacrylate

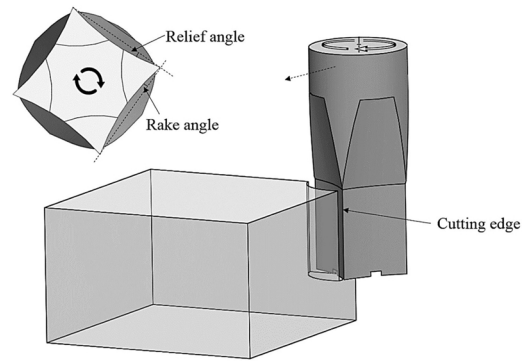


Fig. 1. Micro end mill tool design.

(PMMA)). Cutting tools with 4 cutting edges and a diameter of 100 μm is selected, and the depth of cut per pass is varied from 20 to 60 % of the cutting tool diameter. The performance of the cutting tools is then analyzed in terms of burr formation, surface roughness, surface integrity, and tool condition after machining. To summarize, this paper discusses a novel tool design with high core strength and edge sharpness, introduces a tool fabrication strategy with zero scrap rate, high dimensional accuracy and high repeatability, and analyses the material response in micromilling in terms of burr formation, surface finish and surface defects.

2. Experimental method

At first, 12 micro end mill tools of 100 μm diameter are fabricated using a sequential micro EDM method. These tools are then used for microchannel fabrication on materials with different mechanical properties. The burr characteristics and surface roughness of the machined micro channels are then analyzed with an optical profilometer with 20x magnification (CCI-MP, Taylor and Hobson, UK). It has < 0.2 \AA RMS repeatability, < 0.1 % step height repeatability and 0.1 \AA resolution over the entire measurement range. The surface integrity and tool condition after machining is evaluated using a scanning electron microscope (SEM).

Table 1

Summary of the machining parameters used for micromilling experiments.

Material	Tool dia. (μm) Type	Cutting speed (rpm)	Feed ($\mu\text{m}/$ tooth)	DoC (μm)	$R_a/R_z/S_a$ (μm)	Burr (H or W)*	Reference
Stainless Steel	800/ Two flutes	11936 – 19894	1 – 10	100	–	80 – 120 (H)	[30]
	406/Two flutes	7840	0.05 – 1	30	0.5 – 1 (S_a)	–	[31]
	900/Two flutes	30,000	0.2 – 3.6	50	0.14 – 0.2 (R_a)	–	[32]
Aluminium	508/ Two flutes	120,000	0.25 – 3	50 – 100	0.1 – 0.15 (R_a)	–	[33]
	500/Two flutes	6000 – 36000	0.1 – 1.6	10 – 50	0.07 – 0.08 (R_a)	–	[34]
	100/Single edge	20000 – 60000	0.025 – 0.08	1 – 5	–	–	[35]
	500/Two flutes	6366 – 31831	1 – 6	25	0.028 – 0.086 (R_a)	12.86 – 20.46 (W)	[36]
Copper/Brass	200/Two flutes	35000 – 95000	0.015 – 0.8	10	0.02 – 0.34 (R_a)	30 – 200 (W)	[37]
	25/Special shapes	10000 – 18000	0.0416 – 1.25	0.5 – 1	0.082 – 0.458 (R_a)	–	[29]
	50/ one flute	30,000	1 – 4	5	0.0119 (R_a)	–	[38]
Polymer	500/Two flutes	12000 – 18000	0.4 – 0.1.85	10 – 30	–	10 (W)	[39]
	150 – 600/Two flutes	23873 – 63661	0.1 – 8	20	1.75 – 2.5 (R_z)	–	[40]
	400/Two flutes	20000 – 30000	0.8 – 2.5	200	–	–	[41]
	950/Single Edge	20000 – 100000	0.6 – 3	700	–	–	[42]
	10 – 50/ Special shapes	40000 – 50000	0.1 – 1.2	2 – 10	–	–	[16]

* H for burr height and W for burr width, DoC – Depth of Cut.

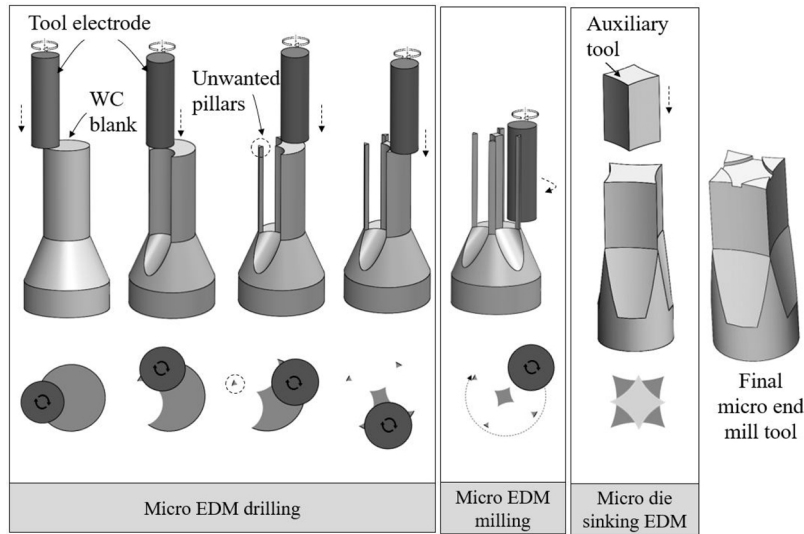


Fig. 2. Steps in micro tool fabrication using sequential micro EDM.

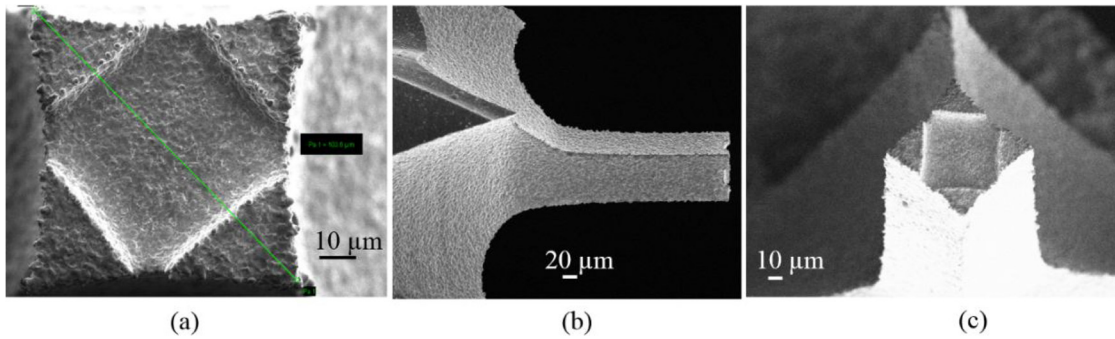


Fig. 3. (a) top view (b) side view and (c) isometric view of the fabricated micro end mill tool.

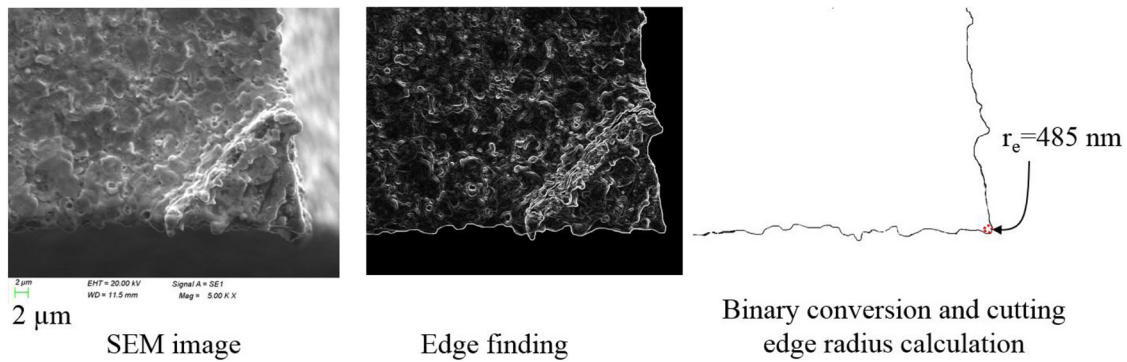


Fig. 4. Edge finding and cutting edge radius calculation by image processing.

Table 2
Mechanical and thermal properties of the workpiece materials.

Properties	Al 6061	Brass 340	AISI 1040	PMMA
Ultimate Tensile strength, (MPa)	210	340	620	62
Yield strength (MPa)	110	115	415	–
Elastic modulus (GPa)	68.9	105	210	3.30
Hardness (MPa)	1049	1177	2069	175
Shear modulus (MPa)	26	39	80	1.70
Poisson's ratio	0.33	0.346	0.3	0.34
Thermal conductivity W/m-K	154	115	24.7	0.209
Coeff. of thermal expansion $\mu\text{m}/\text{m}\cdot^\circ\text{C}$	23.6	20.3	11.3	61

2.1. Tool fabrication

One of the major drawbacks of the earlier tool design is that the tool bottom continuously rubbed with the channel floor surface during machining [28]. To reduce rubbing, material from the tool bottom surface has to be removed without compromising the integrity of cutting edge. A method combining EDM drilling, EDM milling, and die-sinking EDM is employed to fabricate the modified cutting tool. The modified tool design is shown in Fig. 1 and the tool fabrication process is elaborated in Fig. 2. A tool blank (WC) of 1 mm diameter is kept as the workpiece with a positive polarity. A 300 μm WC rod is used as the tool electrode for carving the cutting edges by micro EDM drilling. The drilling process is then followed by a circular EDM milling process to

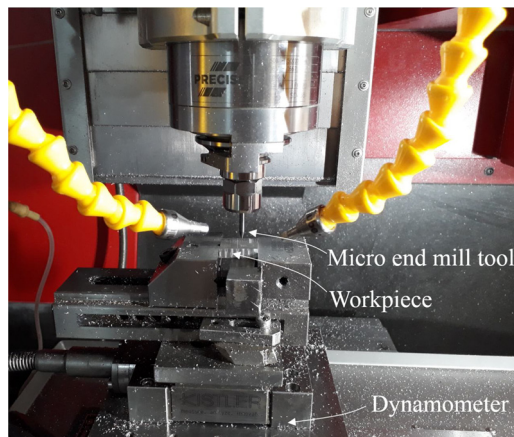


Fig. 5. Set up for micromilling experiments.

Table 3
Machining parameters selected for micromilling experiments.

Machining parameters	
Spindle speed	40,000 RPM
Feed	20 mm/min
Cutting edges	4
Cutting tool diameter	100 μm
Available flute length	300 μm
Length of cut	5 mm
Depth of cut	20, 40, 60 μm

remove unwanted protrusions formed at the corners as shown in Fig. 2. Finally, material from the tool bottom area is removed using die sinking EDM to ensure minimum rubbing and no chip entrapment during machining. The axial alignment of the tool and workpiece is done with the help of a CCD camera and an image analysis software (Motic images plus). The drilling locations are found out using a CAD/CAM tool after incorporating the overcut allowance (to reduce the possible dimensional errors due to overcut during EDM drilling). Optimum EDM parameters for minimum height error and diameter error with the least surface roughness and maximum material removal rate is selected using

the empirical relationships [28]. The voltage is selected as 99 V, capacitance as 1 nF, spindle speed as 2573 rpm and the overcut (for overcut allowance) as 22.5 μm. The possible height error during drilling is compensated by a lengthwise compensation algorithm for blind hole drilling based on image processing [43]. The most challenging part is to make the bottom features on the micro tools. A smaller micro tool of the same shape but of a 70 μm diameter is used as a die-sinking EDM tool electrode and plunged 5 μm into the original cutting tool bottom plane. Before sinking into the cutting tool, the die sinking EDM tool electrode is rotated 45° precisely to align the exit way in the middle of the cutting edge, as shown in Fig. 2. These pathways will reduce the rubbing action and restrict the accumulation of chips in the tool bottom surface. Fig. 3 shown the SEM images of the final tool fabricated by the sequential EDM method. The dimensions of the 12 cutting tools are then analyzed using SEM and found out that the diameter of the tools is in the range of 100 ± 4 μm. For micro end mill tools, another criterion that determines the cutting tool quality is the cutting edge radius. To calculate the edge radius, an image processing algorithm based on the canny edge detection method is employed, and appropriate masks are applied to remove the unwanted areas. The radius of the fitting circle is then calculated to get the cutting edge radius of the micro tool. The procedure of cutting edge radius calculation is shown in Fig. 4. ImageJ software is used to calculate the area of a circle fitting in the cutting edge which is found to varying in between 0.642 μm² to 0.905 μm². The corresponding radius is in the range of 0.452–0.537 μm. The fabricated cutting tools are then used for milling experiments.

3. Method and materials

A 3 axes micro-milling machine (KERN Evo, Germany) is used for milling. The experiments are carried out with the fabricated WC micro end mills tools of 100 μm diameter and 300 μm flute length. 4 workpiece materials are chosen with different mechanical and thermal properties as shown in Table 2. In each experiment, a separate micro end mill tool is used and a microchannel of 5 mm is machined with varying depth of cuts (20 μm, 40 μm, and 60 μm). Two repetitions are performed with each parameter setting. A piezoelectric dynamometer (KISTLER, 9119AA2) is used to measure the cutting forces during the micro milling experiments. The experimental set up for milling experiments is shown in Fig. 5.

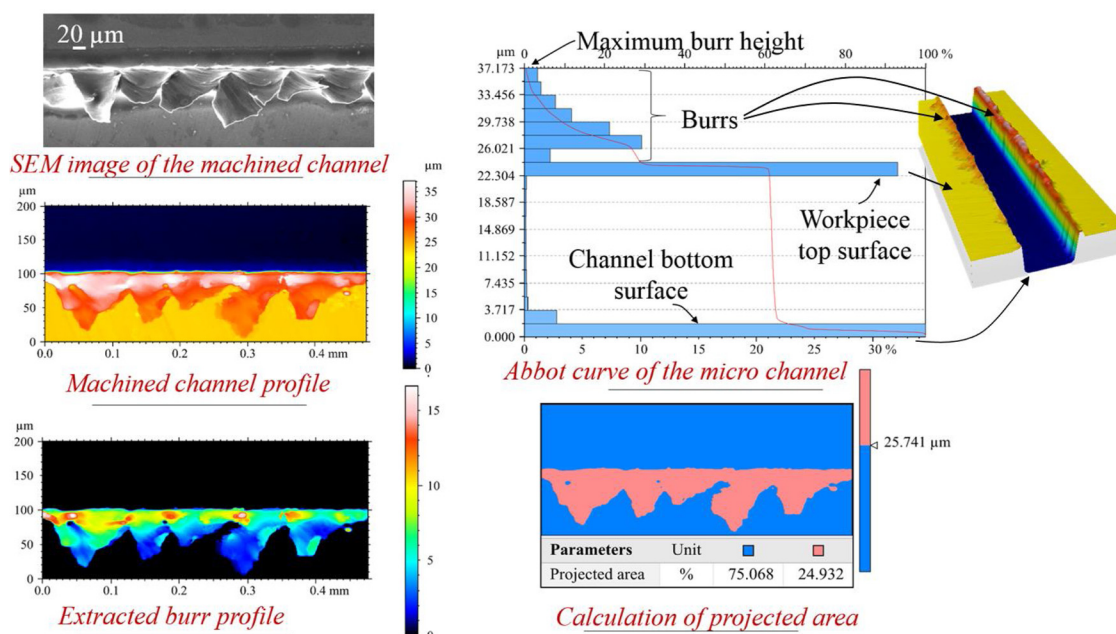


Fig. 6. Procedure for top burr analysis.

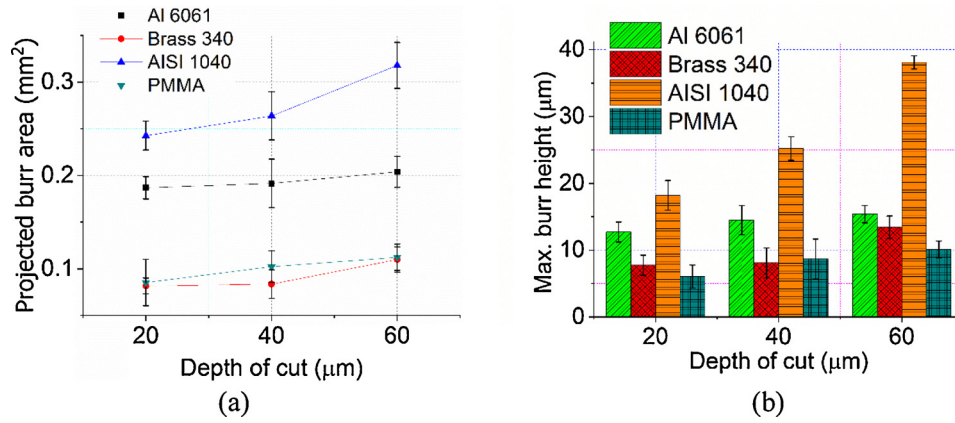


Fig. 7. (a) Projected burr area and (b) maximum burr height of the top burrs in micromilling.

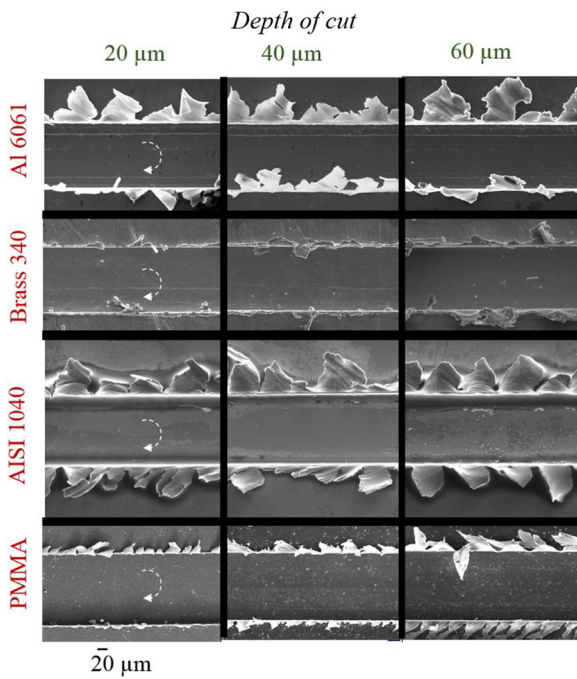


Fig. 8. Top burr profile on different materials at different depth of cuts.

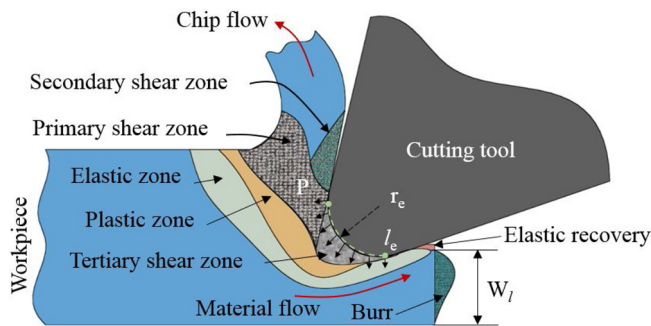


Fig. 9. Mechanism of Poisson burr formation in micromilling.

Machining parameters for the milling experiments are selected to reduce the effects of ploughing and to minimize the impact force on the cutting tool. For that, one of the vital parameter to be determined is the feed per tooth. As the proposed sequential EDM method is successful in fabricating tools of very small cutting edge radius, a smaller feed per tooth can be used. Moreover, as the number of cutting edges increases, the chip load will be shared between four flutes instead of two, which

reduces the hammering action during machining. Spindle speed is selected as 40,000 rpm, and feed is selected as 20 mm/min so that the feed per tooth is 0.125 µm/tooth, which is greater than minimum uncut chip thickness for the selected workpiece materials. The machining parameters are listed in Table 3. Compared to earlier machining experiments listed in Table 1, the depth of cut per pass is very high (20–60 % of the cutting tool diameter).

To analyze the performance of the cutting tools on different materials, the top burr size, surface roughness of the channel bottom surface, and condition of the tool after machining are measured and compared. Usually, characteristics of the micro burrs are analyzed by measuring the width and length of the burrs from an SEM image. This method fails to characterize the burrs along the complete length of the channel as the measuring points are limited to selected sections of the channel. An image processing based method is also used to calculate the total projected burr area [44]. In this paper, instead of relying on an SEM image or an image processing algorithm, the measurements are carried out directly from the optical profilometer, as shown in Fig. 6. Firstly, the different sections of the micro channels (bottom surface, vertical walls, top surface, and burrs) are determined using the abbot curve. These sections are then isolated from each other by finding the threshold height for each. The burrs are then isolated and extracted from the workpiece top surface by determining the threshold height of the top surface and maximum burr height value. The maximum projected area is determined for the up milling side and down milling side separately by slicing at different levels and added together to get the total burr area. As the measurement area is selected as 1 mm² by choosing a section width as 0.2 mm and length of 5 mm (total channel length), the percentage of projected area of the measurement will be equal to the actual projected burr area.

The surface roughness of the channel bottom surface is measured along the longitudinal direction at the center of the microchannel using an optical profilometer. According to Sun et al. [34], the uniformity of the channel bottom surface is also an important parameter to be considered. To determine the surface uniformity of the microchannel surface, surface roughness along the longitudinal direction is determined at different sections with a 5 µm gap (from center of the channels to the side walls).

Surface irregularities in the channel bottom surface of different materials are then analyzed using SEM images to correlate the surface roughness trends with the machining characteristics. Finally, the tool condition after machining is analyzed with the help of SEM images to understand the possible damages on the micro end mill tool during milling.

4. Results and discussion

The fabricated cutting tools are successfully used in micromilling of

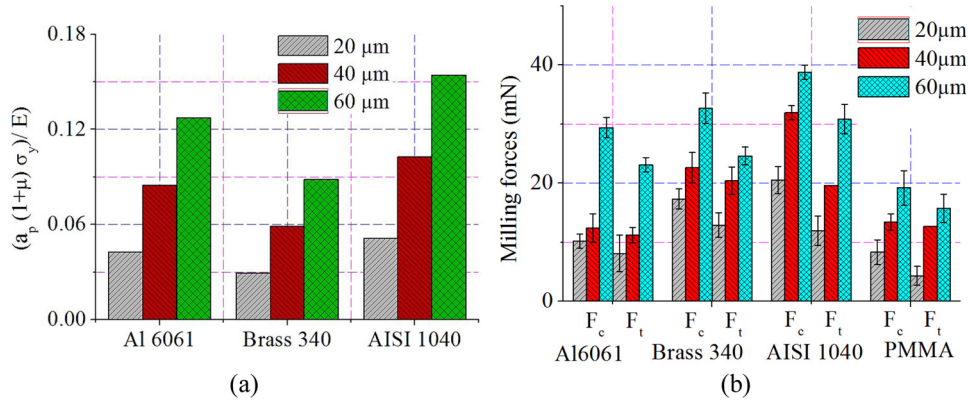


Fig. 10. (a) Ratio of constants in Poisson burr model and (b) force distribution in micromilling of different materials.

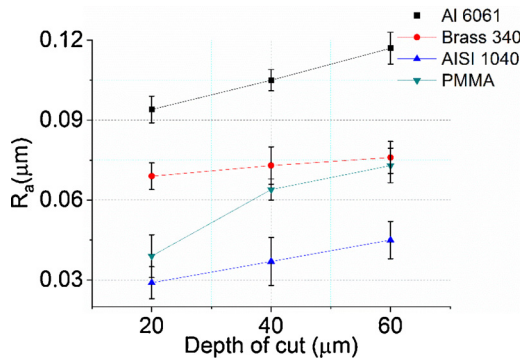


Fig. 11. Variation of surface roughness with respect to the depth of cut.

channels of four different materials. The micromilling tests are then evaluated by studying the burr profile, surface roughness, surface non-uniformity, surface damage and tool damage.

4.1. Burr analysis

The top burr formation along the channel length is analyzed with the help of an optical profilometer. The total projected burr area (sum of burr area in the down milling and up milling side) and the maximum burr height are plotted for all the workpiece materials. As shown in Fig. 7(a), stainless steel shows the maximum burr area followed by aluminium. PMMA and brass show comparatively fewer burrs. Fig. 7(b) shows the variation in the height of the top burrs with respect to materials and depth of cut which follows a similar trend. Fig. 8 shows the SEM images of the micro channels machined at different depths on different materials which confirms the trend visually.

Top burr is a type of Poisson burr formed due to the plastic deformation of workpiece material in sideways during the machining process as shown in Fig. 9. The cutting edge always exerts pressure on the material. As the stress exerted by the bottom section of the cutting edge increases, more of the stagnation material tends to flow sideways [45]. The interactive stress increases with increase in cutting edge radius, amount of elastic recovery of the material, uncut chip thickness and depth of cut. As the volume of material removed during machining increases with the depth of cut, the amount of side flow also increases. Moreover, as the tool plunges deeper into the workpiece material, tool

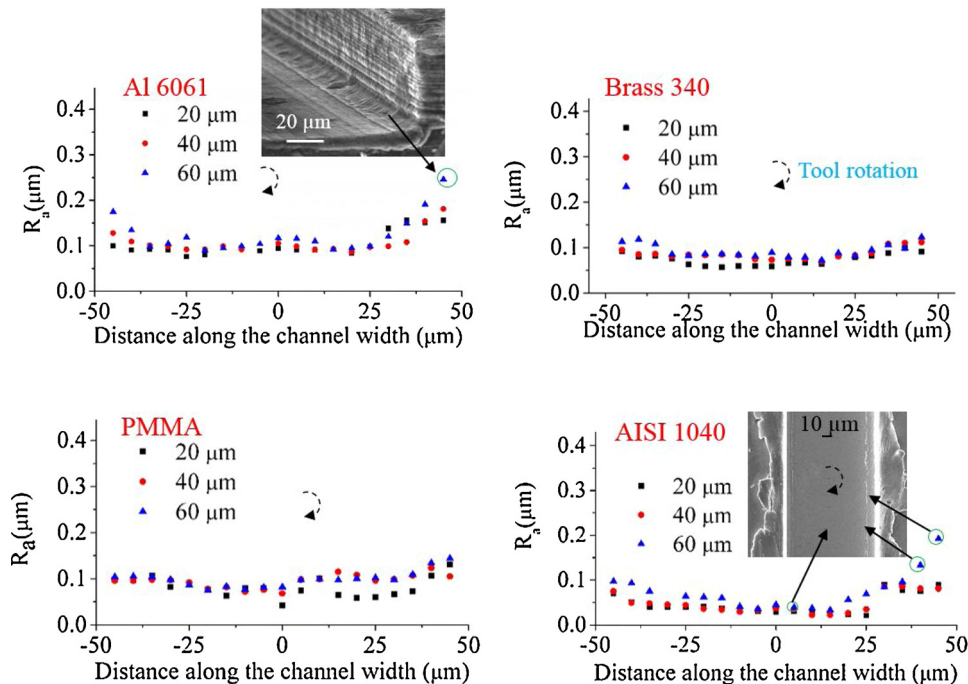


Fig. 12. Surface roughness at different sections of the microchannel width.

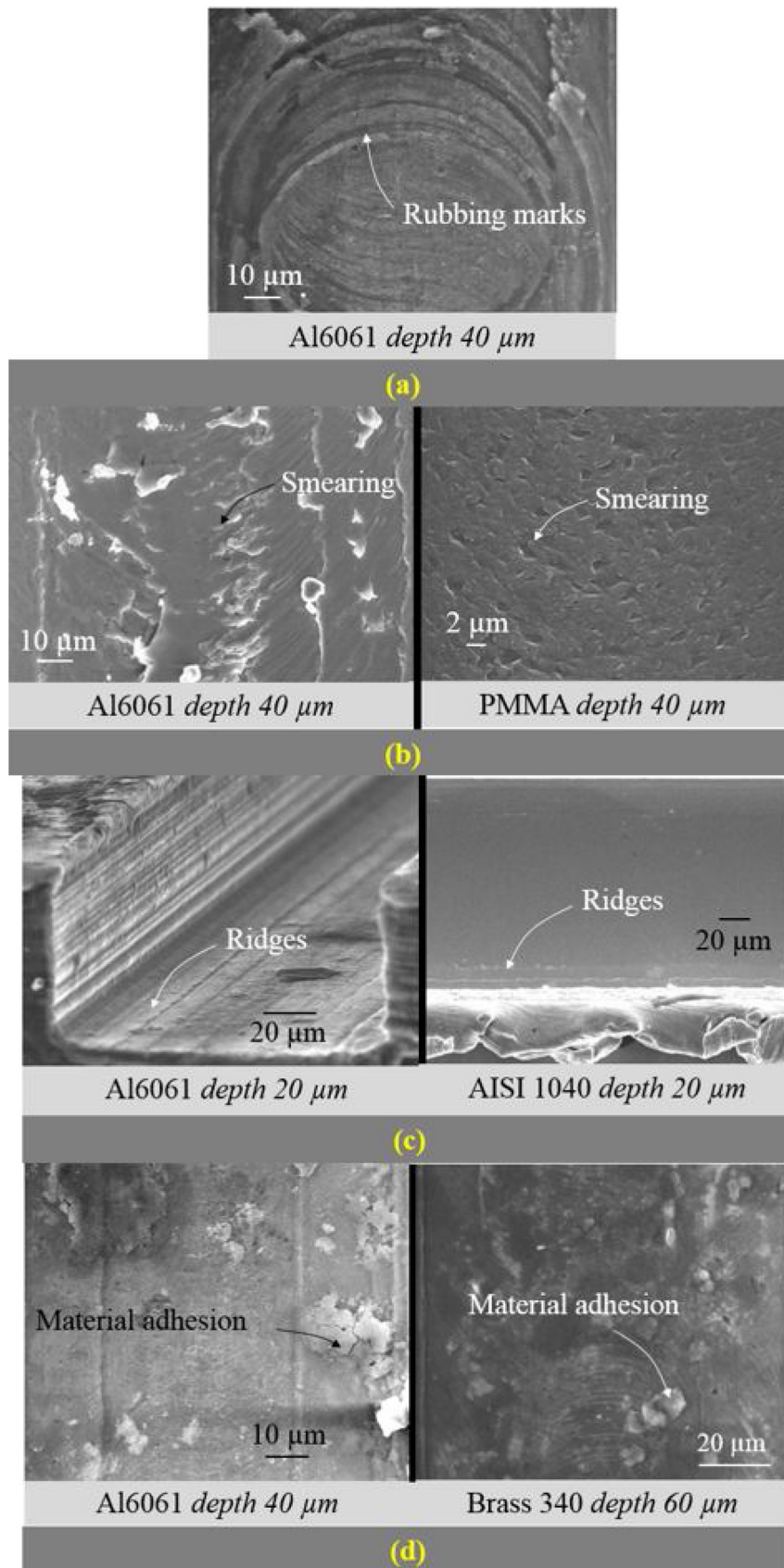


Fig. 13. SEM images of surface damages in the channel bottom surface (a) rubbing marks, (b) smearing, (c) ridge formation and (d) material adhesion to the workpiece surface.

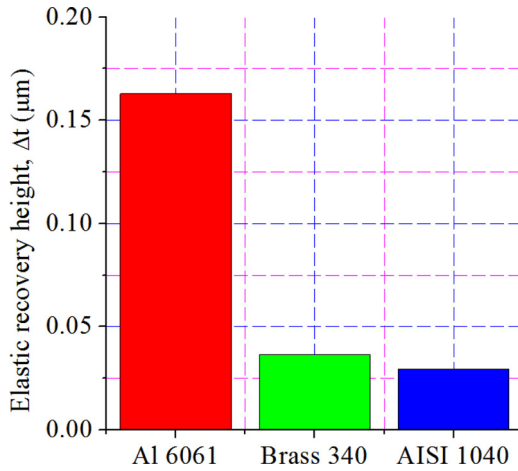


Fig. 14. Height of elastic recovery during micromilling.

vibrations will get severe, and the machining becomes unstable, which leads to larger burrs. This is evident from Fig. 7(a) and (b) that the total burr area and burr height of the top burr is increased with respect to the depth of cut in all materials.

A model for Poisson burr developed by Gillespie and Blotter [46] as shown in Eqs. (1) and (2) are used to understand how the material properties influence the burr formation. The size of the Poisson burr (W_i) can be calculated by Eq. (1) where r_e is the cutting edge radius, \varnothing_a is the state of plastic flow which depends on line force (P) acting on the side walls by the cutting edge and yield stress (σ_y) as given in Eq. (2). Burr size can then be represented as a function of \varnothing_a multiplied by the ratio of material constants. P is the line force acting on the side walls which is a function of the cutting force (F_c), thrust force (F_t), cutting edge radius (r_e) and cutting edge length (l_e). a_p is the depth of cut per pass, μ is the Poisson's ratio, and E is the Young's modulus. To understand the effect of material constants on the size of burrs formed during milling, the ratio of material coefficients in Eq. (1) is plotted for each workpiece materials. Fig. 10(a) shows that aluminum and stainless steel give the maximum material coefficient ratio compared to brass and the ratio increases with the depth of cut. As the model is primarily used for metals and defining yield strength in PMMA is difficult, the model is not applied to the polymer material. Due to the indirect relationship between line force P and the burr length, accessing the effect of P on the burr size is complex. However, according to Gillespie and Blotter [46], as P increases, the burr size also increases. As P is a function of F_c , F_t , r_e and l_e , the magnitude of line force increases with the increase in machining forces and cutting edge radius. From Fig. 10(b), it is clear that the cutting force and thrust during micro milling of stainless steel is much higher than the other three materials and the magnitude

increases with depth of cut. To summarize, during micro milling, burr formation is more is expected to be more in stainless steel, followed by aluminum, brass, and PMMA which also supports the results of the micromilling experiments.

$$W_i = \frac{a_p(1 + \mu)\sigma_y e^{-3\varnothing_a}}{\sqrt{3}E} \left[\frac{-\sin\varnothing}{2(\sqrt{3}\cos\varnothing + \sin\varnothing)} \right] = \frac{a_p(1 + \mu)\sigma_y g(\varnothing_a)}{E\sqrt{3}} \quad (1)$$

where, W_i is the size of the Poisson burr, a_p is the depth of cut per pass, \varnothing_a is the state of plastic flow, σ_y is the yield stress, μ is the Poisson's ratio, and E is the Young's modulus.

$$\varnothing_a = -\sin^{-1}\left(\frac{\sqrt{3}P}{2\sigma_y}\right) + \frac{\pi}{6} \quad (2)$$

where, P is the line force acting on the side walls.

4.2. Surface roughness and surface integrity

From the experiments, the average surface roughness of the channel bottom (along the center line, for the entire channel length) is plotted in Fig. 11. Maximum surface roughness is found on the aluminium micro channels and minimum on the stainless steel. The surface roughness is also affected by the depth of cut in all the materials as the R_a value increases with depth of cut. Surface roughness during micro milling depends on the sharpness of the tool, tool runout, mechanical and thermal properties of the material, feed rate, damping effect induced by the elastic recovery of the workpiece material and the tooltip vibration on the tool [47]. In conventional cutting operations, the lower cutting feed will reduce the surface roughness as the channel bottom will have fine milling marks. However, in micromilling, this phenomenon is overshadowed by the influence of size effect at the lower feed range where the ploughing dominates shearing. The feed per tooth has to be kept higher than the minimum uncut chip thickness to reduce the size effect. However, as the proposed method is capable of fabricating sharper tools, higher surface quality can be maintained at lower feed rate. Moreover, as the number of cutting edges increases, the peak to valley distance is reduced due to back cutting phenomenon. As a result, a nanometer-level surface finish is attained in all the cases as shown in Fig. 11. As the elastic modulus of aluminium is small among the others, higher plastic deformation occurs during machining which makes larger smearing marks on the channel surface. Higher plastic deformation results in more contact area with the cutting tools [48], so that the size effects becomes more influential. Brittle nature of brass and lower shear modulus of PMMA are helped to get smoother machined surfaces compared to aluminium. The higher elastic recovery of aluminium results in rubbing of the tool bottom surface of the trailing edges which also deteriorates the surface quality. From Table 1, Al6061 has maximum thermal conductivity and stainless steel has the

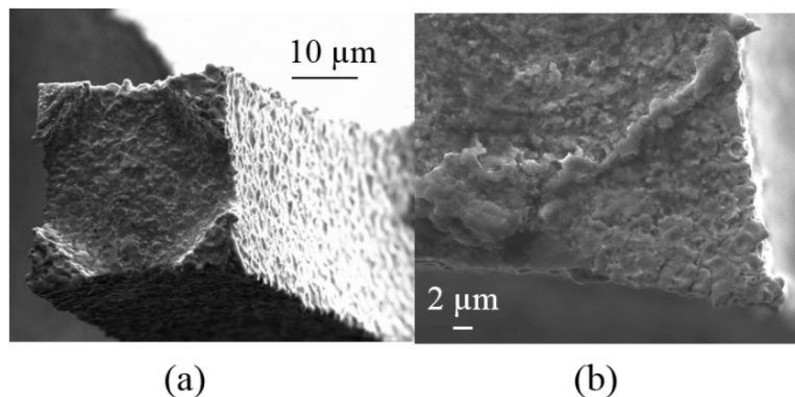


Fig. 15. SEM images of the tool after machining (a) Al-depth 40 μm and (b) brass- depth 20 μm .

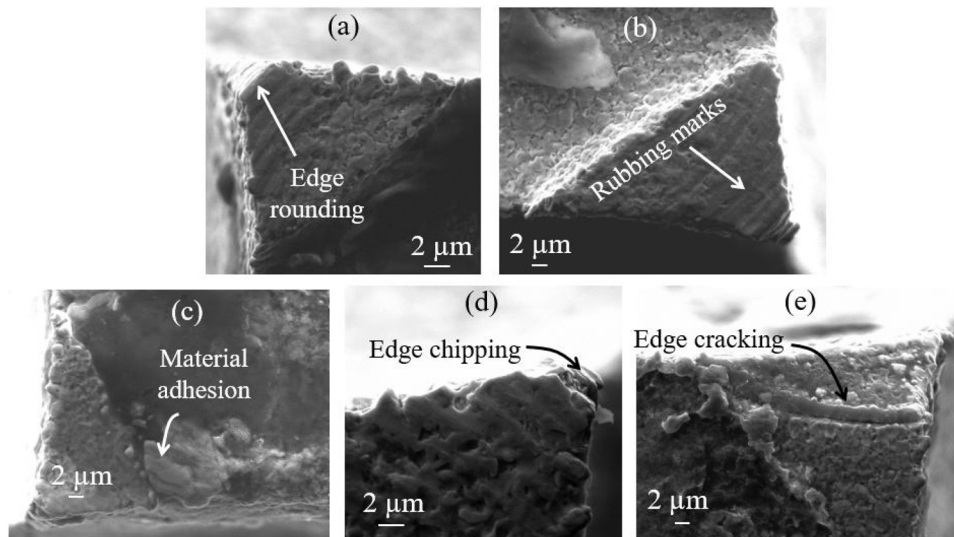


Fig. 16. SEM images of the tools damages due to (a) edge rounding (SS-depth 40 μm) (b) rubbing marks (Al-depth 20 μm) (c) material adhesion (Al-depth 60 μm) (d) edge chipping (SS-depth 40 μm) and (e) edge cracking (brass- depth 40 μm).

minimum. The heat transferred during machining is more accumulated in stainless steel and thermal softening will be maximum. During the machining of aluminum, the thermal softening effect is canceled out in the presence of material strengthening behavior during machining [49]. The increase in surface roughness with respect to depth of cut may be attributed to the increase in instability of the machining process at higher depth of cut.

According to Ahmadi et al. [50], the deformation of the material changes with respect to the tool trajectory due to frequent change over in the mechanism of material removal from ploughing to shearing. The average surface roughness values for different sections along the channel width is measured and compared as shown in Fig. 12. From the analysis of the non-uniformity of surface roughness, it is clear that the roughness values show an increasing trend as it moves from the center of the channel to the side of the channel. Variation in surface roughness is mainly attributed to the change of the machining behavior from shearing to ploughing as it moves from the center of the channel to the sides due to variation in the minimum chip thickness. The size effect also depends on the angle of rotation of the cutting edge, so that maximum variation is visible near to the sides of the channel where uncut chip thickness is minimum. Higher plastic deformation in aluminum and higher edge rounding in stainless steel are some of the reasons for this variation in surface roughness. However, the influence of depth of cut varied randomly along the channel width without any distinguishable trend.

4.3. Surface damages

Surface damages mostly occur due to ploughing and unstable machining. Compared to stainless steel and brass, aluminium showed more surface damages in which rubbing marks (Fig. 13(a)) and smearing (Fig. 13(b)) are dominant. Rubbing marks are formed due to the continuous rubbing of the tool bottom surface with the channel surface. As the elastically recovered material comes in contact with the tool bottom surface, it causes a rubbing action and surface damages. From the equation for calculating the magnitude of elastic recovery (Eq. (3)) during microcutting formulated by Shi [51], it is clear that the thickness of material recovered after machining (Δt) depends on the ratio of the tensile strength (σ_s) and elastic modulus (E) as well as the ratio of material hardness (H) and σ_s . The thickness of the recovered material has a linear relationship with the cutting tool radius (r_c) as well. Putting the material constants listed in Table 1 in Eq. (3), the thickness of elastically recovered material is calculated and plotted in Fig. 14, which

shows that aluminum has a maximum elastic recovery. This might be the reason that the rubbing marks are more evident in aluminum micro channels. The ridge formation, as shown in Fig. 13(c) can be attributed to the accumulation of material pushed away due to ploughing.

Smearing marks are formed due to material ploughing during machining which is higher in aluminum due to more plastic deformation of the material. Adhesive transfer of materials to the channel surface also deteriorates the surface integrity, as shown in Fig. 13(d).

$$\Delta t = \frac{3\sigma_s r_c}{4E} \left[2 \exp\left(\frac{H}{\sigma_s} - \frac{1}{2}\right) - 1 \right] \quad (3)$$

where, Δt is the thickness of material recovered after machining, σ_s is the tensile strength, H is the material hardness, E is the elastic modulus, and r_c is the cutting edge radius.

4.4. Tool damages

Most of the tools retained the sharpness and shape after machining as shown in Fig. 15. “A fresh tool is used for each experiment of 5 mm long channel and the same tool is further used two more times to machine another 5 mm length each time. The tool damages shown in Fig. 16 corresponds to total 15 mm of microchannel length on different materials with different machining conditions.” Some of the tools damaged during machining but none of them were broken completely even the depth of cut per pass was up to 60 % of the tool diameter. Retention of the tool integrity of most of the tools confirms the superior tool rigidity of the proposed tool design. Edge rounding and rubbing marks are the predominant tool defects in the proposed tools. Fig. 16(a) shows the rounding of cutting edges mostly happened in micromilling on stainless steel. Fig. 16(b) shows the rubbing marks due to the contact between the tool bottom surface and the channel floor. These marks are more evident in cutting tools used for aluminium machining which confirms the effect of elastic recovery on the rubbing phenomenon as stated previously. Fig. 16(c) shows material deposition of the tool predominantly present in aluminium machining. Fig. 16(d) shows edge chipping where a chunk of material from the cutting edge tip is chipped out during machining. Fig. 16(e) shows crack formation at the cutting edge which may lead to tool fracture as machining progresses.

5. Conclusions

Machining experiments are performed at different depth of cut on

different materials and performance is compared with reference to burr formation, surface roughness, surface damage, and tool damage.

- The characteristics of top burr formation are studied by a burr quantification method based on optical profilometer. Largest burrs are generated on AISI 1040 and aluminium.
- The surface roughness analysis revealed that the tool is capable of fabricating micro channels with nanometer-level surface finish in all the workpiece materials.
- Surface uniformity analysis showed that the surface roughness varies along the channel width due to the increased ploughing near to the channel sidewalls.
- Analysis of the channel surface integrity revealed that the reduced surface roughness in aluminium is attributed to rubbing marks, smearing, and material adhesion in the channel bottom surface.
- Examining the tool condition after milling showed the possible tool damages in the proposed micro end mill tool.

Declaration of Competing Interest

The authors declare that they have no known competing financial interests or personal relationships that could have appeared to influence the work reported in this paper.

Acknowledgements

The authors acknowledge the funding support from the Institute under SGDRGrant, and Science and Engineering Research Board (SERB) under young scientist scheme (YSS/2015/001163).

References

- [1] Sohn JM, Byun YC, Cho JY, Choe J, Song KH. Development of the integrated methanol fuel processor using micro-channel patterned devices and its performance for steam reforming of methanol. *Int J Hydrogen Energy* 2007;32:5103–8.
- [2] Cai W, Wang F, Van Veen A, Descorme C, Schuurman Y, Shen W, et al. Hydrogen production from ethanol steam reforming in a micro-channel reactor. *Int J Hydrogen Energy* 2010;35:1152–9.
- [3] Luo X, Liu Y, Liu W. A honeycomb microchannel cooling system for microelectronics cooling. *Heat Transf Eng* 2011;32:616–23.
- [4] Lim SS, Kim YT, Kang CG. Fabrication of aluminum 1050 micro-channel proton exchange membrane fuel cell bipolar plate using rubber-pad-forming process. *Int J Adv Manuf Technol* 2013;65:231–8.
- [5] Nguyen N-T, Wu Z. Micromixers-a review. *J Micromech Microeng* 2004;15:R1.
- [6] Adams AA, Okagbare PI, Feng J, Hupert ML, Patterson D, Göttert J, et al. Highly efficient circulating tumor cell isolation from whole blood and label-free enumeration using polymer-based microfluidics with an integrated conductivity sensor. *J Am Chem Soc* 2008;130:8633–41.
- [7] Trotta G, Volpe A, Ancona A, Fassi I. Flexible micro manufacturing platform for the fabrication of PMMA microfluidic devices. *J Manuf Process* 2018;35:107–17. <https://doi.org/10.1016/j.jmapro.2018.07.030>.
- [8] Gattass RR, Mazur E. Femtosecond laser micromachining in transparent materials. *Nat Photonics* 2008;2:219.
- [9] Au AK, Lee W, Folch A. Mail-order microfluidics: evaluation of stereolithography for the production of microfluidic devices. *Lab Chip* 2014;14:1294–301.
- [10] Hutchison JB, Haraldsson KT, Good BT, Sebra RP, Luo N, Anseth KS, et al. Robust polymer microfluidic device fabrication via contact liquid photolithographic polymerization (CLiPP). *Lab Chip* 2004;4:658–62.
- [11] Hnatovsky C, Taylor RS, Simova E, Bhardwaj VR, Rayner DM, Corkum PB. Polarization-selective etching in femtosecond laser-assisted microfluidic channel fabrication in fused silica. *Opt Lett* 2005;30:1867–9.
- [12] Mittal RK, Kulkarni SS, Singh RK. Effect of lubrication on machining response and dynamic instability in high-speed micromilling of Ti-6Al-4V. *J Manuf Process* 2017;28:413–21. <https://doi.org/10.1016/j.jmapro.2017.04.007>.
- [13] Arif M, Rahman M, San WY. An experimental investigation into micro ball end-milling of silicon. *J Manuf Process* 2012;14:52–61. <https://doi.org/10.1016/j.jmapro.2011.09.004>.
- [14] Li P, Oosterling JAJ, Hoogstrate AM, Langen HH, Munnig Schmidt RH. Design of micro square endmills for hard milling applications. *Int J Adv Manuf Technol* 2011;57:859–70. <https://doi.org/10.1007/s00170-011-3330-6>.
- [15] Cheng X, Wang Z, Nakamoto K, Yamazaki K. A study on the micro tooling for micro/nano milling. *Int J Adv Manuf Technol* 2011;53:523–33. <https://doi.org/10.1007/s00170-010-2856-3>.
- [16] Aurich JC, Reichenbach IG, Schüler GM. Manufacture and application of ultra-small micro end mills. *CIRP Ann Manuf Technol* 2012;61:83–6. <https://doi.org/10.1016/j.cirp.2012.03.012>.
- [17] Kang IS, Kim JS, Seo YW. Investigation of cutting force behaviour considering the effect of cutting edge radius in the micro-scale milling of AISI 1045 steel. *Proc Inst Mech Eng Part B J Eng Manuf* 2011;225:163–71. <https://doi.org/10.1243/09544054JEM1762>.
- [18] Malekian M, Mostofa MG, Park SS, Jun MBG. Modeling of minimum uncut chip thickness in micro machining of aluminum. *J Mater Process Technol* 2012;212:553–9. <https://doi.org/10.1016/j.jmatprotec.2011.05.022>.
- [19] Ding X, Lim GC, Cheng CK, Butler DL, Shaw KC, Liu K, et al. Fabrication of a micro-size diamond tool using a focused ion beam. *J Micromech Microeng* 2008;18. <https://doi.org/10.1088/0960-1317/18/7/075017>.
- [20] Nakamoto K, Katahira K, Ohmori H, Yamazaki K, Aoyama T. A study on the quality of micro-machined surfaces on tungsten carbide generated by PCD micro end-milling. *CIRP Ann Manuf Technol* 2012;61:567–70. <https://doi.org/10.1016/j.cirp.2012.03.112>.
- [21] Fleischer J, Deuchert M, Ruhs C, Kühlewein C, Halvadjysky G, Schmidt C. Design and manufacturing of micro milling tools. *Microsyst Technol* 2008;14:1771–5. <https://doi.org/10.1007/s00542-008-0652-x>.
- [22] Perveen A, San WY, Rahman M. Fabrication of different geometry cutting tools and their effect on the vertical micro-grinding of BK7 glass. *Int J Adv Manuf Technol* 2012;61:101–15. <https://doi.org/10.1007/s00170-011-3688-5>.
- [23] Picard YN, Adams DP, Vasile MJ, Ritchey MB. Focused ion beam-shaped microtools for ultra-precision machining of cylindrical components. *Precis Eng* 2003;27:59–69. [https://doi.org/10.1016/S0141-6359\(02\)00188-5](https://doi.org/10.1016/S0141-6359(02)00188-5).
- [24] Morgan CJ, Vallance RR, Marsh ER. Micro machining glass with poly crystalline diamond tools shaped by micro electro discharge machining. *J Micromech Microeng* 2004;14:1687–92. <https://doi.org/10.1088/0960-1317/14/12/013>.
- [25] Zhang Z, Peng H, Yan J. Micro-cutting characteristics of EDM fabricated high-precision polycrystalline diamond tools. *Int J Mach Tools Manuf* 2013;65:99–106. <https://doi.org/10.1016/j.ijmachtools.2012.10.007>.
- [26] Cheng X, Wang Z, Nakamoto K, Yamazaki K. Design and development of PCD micro straight edge end mills for micro/nano machining of hard and brittle materials. *J Mech Sci Technol* 2010;24:2261–8. <https://doi.org/10.1007/s12206-010-0804-7>.
- [27] Fonda P, Katahira K, Kobayashi Y, Yamazaki K. WEDM condition parameter optimization for PCD microtool geometry fabrication process and quality improvement. *Int J Adv Manuf Technol* 2012;63:1011–9. <https://doi.org/10.1007/s00170-012-3977-7>.
- [28] Malayath G, Sidpara AM, Deb S. Fabrication of micro-end mill tool by EDM and its performance evaluation. *Mach Sci Technol* 2019;0:1–26. <https://doi.org/10.1080/10910344.2019.1636269>.
- [29] Adams DP, Vasile MJ, Benavides G, Campbell AN. Micromilling of metal alloys with focused ion beam-fabricated tools. *Precis Eng* 2001;25:107–13. [https://doi.org/10.1016/S0141-6359\(00\)00064-7](https://doi.org/10.1016/S0141-6359(00)00064-7).
- [30] Lopes Mougo A, de Oliveira Campos F, Araujo AC. Mechanistic study on micro-milling of the super duplex stainless steel UNS S32750. *J Manuf Process* 2018;34:31–9. <https://doi.org/10.1016/j.jmapro.2018.05.017>.
- [31] Wang Z, Kovvuri V, Araujo A, Bacci M, Hung WNP, Bukkapatnam STS. Built-up-edge effects on surface deterioration in micromilling processes. *J Manuf Process* 2016;24:321–7. <https://doi.org/10.1016/j.jmapro.2016.03.016>.
- [32] Aramcharoen A, Mativenga PT. Size effect and tool geometry in micromilling of tool steel. *Precis Eng* 2009;33:402–7. <https://doi.org/10.1016/j.precisioneng.2008.11.002>.
- [33] Bissacco G, Hansen HN, De Chiffre L. Micromilling of hardened tool steel for mould making applications. *J Mater Process Technol* 2005;167:201–7. <https://doi.org/10.1016/j.jmatprotec.2005.05.029>.
- [34] Sun Z, To S, Zhang S, Zhang G. Theoretical and experimental investigation into non-uniformity of surface generation in micro-milling. *Int J Mech Sci* 2018;140:313–24. <https://doi.org/10.1016/j.ijmecsci.2018.03.019>.
- [35] Chern GL, Wu YJE, Cheng JC, Yao JC. Study on burr formation in micro-machining using micro-tools fabricated by micro-EDM. *Precis Eng* 2007;31:122–9. <https://doi.org/10.1016/j.precisioneng.2006.04.001>.
- [36] Kumar AS, Deb S, Paul S. A study on micro-milling of aluminium 6061 and copper with respect to cutting forces, surface roughness and burr formation. *ASME 2018 13th Int Manuf Sci Eng Conf MSEC 2018 4*. 2018. p. 1–7. <https://doi.org/10.1115/MSEC2018-6570>.
- [37] Kiswanto G, Zariatin DL, Ko TJ. The effect of spindle speed, feed-rate and machining time to the surface roughness and burr formation of Aluminum Alloy 1100 in micro-milling operation. *J Manuf Process* 2015;16:435–50. <https://doi.org/10.1016/j.jmapro.2014.05.003>.
- [38] Aurich JC, Bohley M, Reichenbach IG, Kirsch B. Surface quality in micro milling: influences of spindle and cutting parameters. *CIRP Ann* 2017;66:101–4.
- [39] Liu Y, Li P, Liu K, Zhang Y. Micro milling of copper thin wall structure. *Int J Adv Manuf Technol* 2017;90:405–12. <https://doi.org/10.1007/s00170-016-9334-5>.
- [40] Takács M, Verő B, Mészáros I. Micromilling of metallic materials. *J Mater Process Technol* 2003;138:152–5. [https://doi.org/10.1016/S0924-0136\(03\)00064-5](https://doi.org/10.1016/S0924-0136(03)00064-5).
- [41] Kuram E. Micro-milling of unreinforced and reinforced polypropylene. *Proc Inst Mech Eng Part B J Eng Manuf* 2017;0954405417711737. <https://doi.org/10.1177/0954405417711737>.
- [42] Irvine P, O'Donnell GE, Walsh B. Fundamental investigations into burr formation and damage mechanisms in the micro-milling of a biomedical grade polymer. *Mach Sci Technol* 2015;19:112–33.
- [43] Malayath G, Katta S, Sidpara AM, Deb S. Length-wise tool wear compensation for micro electric discharge drilling of blind holes. *Measurement* 2018;134:888–96. <https://doi.org/10.1016/j.measurement.2018.12.047>.
- [44] Medeossi F, Sorgato M, Bruschi S, Savio E. Novel method for burrs quantitative evaluation in micro-milling. *Precis Eng* 2018;54:379–87. <https://doi.org/10.1016/j.precisioneng.2018.05.001>.

- j.precisioneng.2018.07.007.
- [45] Krui S, Aoyama H, Ohta K, Sano N. Prediction of thickness and height of burr based on burr formation mechanisms in end milling. *J Adv Mech Des Syst Manuf* 2014;8.
- [46] Gillespie LK, Blotter PT. The formation and properties of machining burrs. *J Inst Eng* 1976;98:66–74.
- [47] Wang H, To S, Chan CY, Cheung CF, Lee WB. A theoretical and experimental investigation of the tool-tip vibration and its influence upon surface generation in single-point diamond turning. *Int J Mach Tools Manuf* 2010;50:241–52.
- [48] Zhang J, Feng C, Wang H, Gong Y. Analytical investigation of the micro groove surface topography by micro-milling. *Micromachines* 2019;10:582.
- [49] Yuan ZJ, Zhou M, Dong S. Effect of diamond tool sharpness on minimum cutting thickness and cutting surface integrity in ultraprecision machining. *J Mater Process Technol* 1996;62:327–30.
- [50] Sun Z, To S, Zhang S, Zhang G. Theoretical and experimental investigation into non-uniformity of surface generation in micro-milling. *Int J Mech Sci* 2018;140:313–24.
- [51] Shi WT. *Micro cutting technology* 2011. Beijing: China Machine Press; 2011.